The role of CO* as a spectator in CO2 electro-reduction on RuO2

Bhowmik, Arghya; Hansen, Heine Anton; Vegge, Tejs

Published in:
The Journal of Physical Chemistry Part C

Link to article, DOI:
10.1021/acs.jpcc.7b04242

Publication date:
2017

Document Version
Peer reviewed version

Article

The role of CO* as a spectator in CO electro-reduction on RuO

Arghya Bhowmik, Heine Anton Hansen, and Tejs Vegge

J. Phys. Chem. C, **Just Accepted Manuscript** • DOI: 10.1021/acs.jpcc.7b04242 • Publication Date (Web): 02 Aug 2017

The Role of CO* as a Spectator in CO_2 Electro-reduction on RuO_2

Arghya Bhowmik, Dr. Heine Anton Hansen and Prof. Dr. Tejs Vegge*

Department of Energy Conversion and Storage, Technical University of Denmark, Fysikvej Bldg. 309,

DK-2800 Kgs. Lyngby, Denmark.

E-mail: teve@dtu.dk; Fax: +45 46 77 57 58; Tel: +45 45 25 82 01

Abstract:

RuO_2 based electrocatalysts are found to be active at low over-potential towards direct electrochemical reduction of CO_2 to formic acid and methanol. RuO_2 can circumvent the thermodynamic bottleneck resulting from the scaling relations observed on metallic electrocatalyst, by employing an alternate pathway through oxygen-coordinated intermediates. Employing density functional theory based computational electrocatalysis models we show adsorbate-adsorbate interaction effects for adsorbates and reaction intermediates on the RuO_2(110) surface are large and impactful to the reaction thermodynamics. We studied binding energy amendment due to adsorbate interaction (steric and electronic) with varying coverage of CO spectators on the catalyst surface. Implications on the reaction pathways help us rationalize differences in experimentally observed carbonaceous product mix and suppression of the hydrogen evolution reaction (HER). We show that a moderate CO* coverage (~50%) is necessary for obtaining methanol as a product and that higher CO* coverages leads to very low overpotential for formic acid evolution. Our analysis also clarifies the importance of the reaction condition for CO_2 reduction to liquid fuels utilizing RuO_2 based electrocatalysts.*

1. Introduction

The last hundred years of relentless human development have relied on fossil fuel based energy resources. To translate into a sustainable alternative course of long term growth[1], expanding renewable energy resources must be tapped at the earliest possible time. This is to mitigate limitations of fossil fuel as well as the inherent environmental problems emanating from increased anthropogenic emissions of CO_2. An electricity grid brimming with renewable electricity from wind and solar plants or

cars propelled by renewable energy depends on inexpensive energy conversion and storage technologies[2]. Electrochemical reduction of carbon dioxide to liquid fuels is an appealing approach that could alleviate much of the CO_2 emission challenge, solve the bottleneck of cheap energy storage and penetrate the fossil fuel dependent transport sector[3].

The main challenge of direct electrochemical reduction of CO_2 to fuel molecules like formic acid, methanol or methane, is the absence of stable catalysts that can enable the CO_2 reduction reaction (CO2RR) at low overpotential and high selectivity over the hydrogen evolution reaction (HER)[4,5]. The underlying chemistry limiting the effectiveness of metallic catalysts in CO2RR to methane or methanol was recently ascertained through density functional theory based modeling of the thermodynamics of reaction steps involved[6]. Adsorbed CO (CO*) is a crucial reaction intermediate in the CO2RR pathway on metallic catalysts. Strong correlation between the binding energy of key intermediates CO* and CHO* on metal catalyst surfaces enforces a large potential requirement for CO2RR to methane irrespective of the CO* binding energy of the metal[7]. Thus, further reduction of CO* remains a bottleneck for metal catalysts. Only copper produces mixtures of methane, ethane and formic acid at high overpotential, owing to its favorable position in the theoretical activity volcano proposed in previous work. Ruthenium oxide based electrocatalysts have been repeatedly shown[8–10] to produce methanol from CO_2 with up to 60% Faradic Efficiency (FE) at low overpotential. Formic acid has been reported[11] to be the other major CO2RR product on RuO_2 based electrocatalysts. While experimental results have been very affirmative towards good CO2RR activity, oxide catalysts have largely been overlooked amidst the recent spurt in scientific activity pertaining to electrocatalytic route to CO_2 reduction[12–18]. Our previous work on RuO_2-based electrocatalysts for CO_2 reduction[19] explained that a different reaction mechanism involving HCOOH* intermediate instead of CO* is active on oxide electrocatalysts. We have also established[20] that different sets of scaling laws and resulting activity volcano leads to lower thermodynamic barriers for the CO_2 conversion reaction than their metal counterparts. This behavior emanates from the fundamentally different reaction path followed on oxide catalysts compared to metal catalysts. CO_2 activation on metals lead to COOH* intermediate and consecutive protonation to reaction intermediates like CO*, CHO*/COH*, CHOH*/H_2CO* which tend to bind to the metal through the carbon atom[21,22]. On RuO_2 (110), CO_2 activation leads to OCHO*, which is further reduced to HCOOH*, H2COOH etc, which bind to the catalyst through oxygen atoms[19]. The different reaction pathway signify different scaling relations govern CO2RR on oxide surfaces[20]. In particular, the limitation from the CO*/CHO* scaling is avoided.

The presence of spectator species on the catalyst surface can enhance or poison electrocatalyst activity, as have been studied theoretically and experimentally[23–27]. Despite the COOH* intermediate being much less stable than the OCHO* intermediate, a small amount of COOH* might form on CO_2 activation. Further

reduction is expected to leave adsorbed CO* from this contingent reaction[11]. CO* spectators interact with other adsorbed reaction intermediates and alter their binding energy. We have observed that spectator CO* species can have large effect on H* binding free energy, potentially promoting/poisoning HER[20]. Similar behavior has been observed for metallic catalysts[28]. We expect similar effect can be present for OH* binding free energy as well. Intermediates formed during CO2RR to methanol on the RuO_2 catalyst surface are bound to the surface by oxygen atoms, and their binding energy is correlated with the OH* binding energy. Thus a strong effect of CO* spectators on the onset potential for methanol production and selectivity over HER is expected. Shift in the reaction site of CO2RR due to blockade of more favorable sites by CO* spectator can have very large effect on the thermodynamics of elementary reaction steps. For example, under reducing conditions the RuO_2(110) surface can have both strong biding bridge sites and weak binding coordinated unsaturated (cus) sites available for intermediates. If all bridge sites (br) are occupied by spectator CO* species, then the reaction can only proceed through cus sites. To create a categorical understanding of CO* spectators on the CO2RR pathway on RuO_2(110) surface, we study the possible reaction intermediate and paths to formic acid, methanol and methane in the presence of different concentrations of CO* spectators as well as variation in the br/cus sites occupied by spectator CO*. This work displays that weakening and strengthening of binding energies is of surprising importance towards both onset potential and possibly also the product selectivity for CO2RR on RuO_2. The outcome from this study is especially important to the understanding and development of oxide-based CO_2RR electrocatalyst, which may break the scaling relations. We show that high CO* coverage can render RuO_2 based catalysts very effective at formic acid evolution and lower selectivity towards HER, while a moderate coverage improves on methanol selectivity. Our results might give a clue to the widely varied product composition obtained from CO2RR with RuO_2 based electrocatalysts and highlight the importance of spectator coverage for successful CO2RR using RuO_2.

2. Computational details

We utilize VASP[29] package for density functional theory (DFT) based simulation of model catalyst surfaces with adsorbed reaction intermediates. Standard PBE-PAW potentials as distributed with VASP 5.3 are used with 500 eV wavefunction cutoff. Previous comparison study on convergence of chemisorption energy on RuO_2 surface from VASP (PAW) and Wien2K (all electron) indicated that 400 eV cutoff is sufficient for routine calculations. 600 eV cutoff for standard PAW can provide accuracy of up to 10 meV [30]. Higher energy cutoff for this work is irrelevant as errors in the order of 0.1 eV is expected in GGA level theory[31]. Here newly developed BEEF-vdW[32] exchange correlation functional is utilized. Our lattice parameter estimates are a=4.537 Å and c=3.135 Å for RuO_2, which agrees well with experimental data[33]. Following our previous studies[19,20] the supercell representing

the catalyst surface RuO_2(110) consists of a four layer thick slab with lower two layers fixed at atomic positions identical to bulk RuO_2. The bridge site is considered vacant due to reducing environment during CO2RR (Figure SI1). This model has two bridge and two cus sites available for reaction intermediates and spectator CO* molecules. During simulation, we use a 4x4x1 k-point mesh and 16 Å of vacuum in the z-direction and Gaussian electronic smearing. Optimization of atomic positions are done until forces on atoms in top two layers and adsorbates are lower than 0.003 eV/Å. Vibrational modes for adsorbed molecules are also analyzed to enable finite temperature free energy estimates by approximating adsorbate degrees of freedom as independent quantum mechanical harmonic oscillators (Table SI1).
Adsorbate binding free energies are estimated w.r.t. gas phase free energies (Table SI2) of hydrogen, water and CO_2 [20]. Systematic DFT-errors in total energy evaluation are corrected for H_2 (0.1 eV), CO_2 (0.3 eV), formic acid (0.15 eV) and COOH* (0.15 eV) following the approach by Christensen et al.[34]. A stabilization of formic acid in solution[35] from deprotonation in neutral electrolyte (-0.19 eV) is also taken into account, and the experimentally observed reaction product concentrations were used for free energy estimation of methanol[9], formic acid and methane[11] free energies. The reaction thermodynamics calculations are susceptible to variation in reactant/product concentration in the electrolyte. High concentration of methanol in electrolyte leads to increased free energy (up to 0.2 eV) and release of methanol might become difficult. The low vapor pressure of formic acid means small variation in free energy from higher concentration. Thus, effects of concentration are minimal for formic acid evolution.

Vibrational modes of adsorbate molecules are used to estimate zero-point energy, heat capacity and entropic contributions to the free energy at room temperature using the harmonic oscillator model as implemented in atomistic simulation environment (ASE). Usage of the reversible hydrogen electrode (RHE) scale for electrochemical potential helps simplify onset potential estimation by considering reversible formation of a proton/electron pair from a hydrogen molecule as zero V-RHE at any given pH. Accordingly, the analysis becomes pH independent except for the free energy of formic acid in solution. We have employed the computational hydrogen electrode (CHE) model[36] to determine the thermodynamics of the electrochemical reaction steps involving single electron/proton transfer. The free energy of an adsorbate formed at the n^{th} proton transfer step if lowered by nU eV when a potential of U vs. RHE (V-RHE) is applied. Under the assumptions of the CHE model, for a particular, elementary proton transfer step, requiring an increase in binding free energy can be made free energy neutral by applying a negative potential, equivalent to the increase in free energy at 0 V-RHE. Hence, an analysis of relative binding energies of adsorbates formed at different electron transfer steps (Table 1) at 0 V-RHE allows us to investigate modifications in CO2RR pathway and onset potential as well as selectivity over HER due to adsorbate interactions with CO*.

Table 1: Adsorbate/product cases examined at electron transfer step from 0e$^-$ to 8e$^-$

0e$^-$	1 e$^-$	2 e$^-$	3 e$^-$	4 e$^-$
*	OCHO*, H*, COOH*	HCOOH*, CO*+H_2O(l), HCOOH(aq), H_2(aq)	H_2COOH*	H_3CO*+OH*, H_2CO+ H_2O(l), O*+CH_3OH(aq)
5 e$^-$	6 e$^-$	7 e$^-$	8 e$^-$	
H_3CO*+ H_2O(l), H_2COH*+ H_2O(l), OH*+CH_3OH(aq)	O*+CH_4(aq)+ H_2O(l), CH_3OH*+ H_2O(l), CH_3OH(aq)+H_2O(l)	OH*+CH_4(aq) + H_2O(l)	CH_4(aq)+ H_2O(l)	

3. Results and discussion

3.1. Spectator coverage

With four adsorption sites in the simulation model (Figure SI1), CO* coverage can be 0%, 25%, 50%, 75% or 100%, respectively. Each CO* spectator in the simulation model amounts to 25% added CO* coverage. With full CO* coverage, CO2RR or HER cannot advance due to unavailability of active sites, unless CO* is first reduced. Two different types of active site being present and considering symmetry of the relative positions of the CO* adsorbates, 25% and 75% coverage can be realized in two different ways, while 50% coverage leads to four different representations (Figure SI2). All such different CO* coverages are inspected for their relative thermodynamic stability (Figure SI3). Visual representations are provided in Figure SI2.

On the bare surface, the 1st CO* adsorption at the bridge site is favorable compared to cus site by 0.18 eV (Figure SI3). With respect to the CO molecule, the binding free energy of CO* at the bridge site of the bare surfaces is -1.34 eV. Two cus sites and one bridge site are accessible for catalysis at 25% CO* coverage. With 50% CO* coverage, putting all adsorbates in the bridge site is the most stable configuration. All other cus configurations with 50% CO* coverage are less stable by 0.28 eV. The adsorption free energy for the two 50% CO* coverage configurations with a combination of bridge and cus occupancy are less stable than the all bridge configuration by 0.08 eV (while neighboring bridge and cus sites have CO* (bridge+cus-near in SI3)) and 0.1 eV (occupied bridge and cus sites are far apart (bridge+cus-far in SI3)). With both bridge sites covered by CO*, catalysis can only occur on the cus sites available (Figure SI2). On the other hand, if CO at 50% CO* coverage occupies both bridge and cus sites, there are still bridge and cus sites available for CO2RR. At 75% CO* coverage, the adsorbate configuration with CO*

on 2*bridge+cus sites is more stable than CO* on bridge+2*cus by 0.2 eV (Figure SI3). These two configurations are fundamentally different, as the first allows catalysis through the cus sites and the latter requires the reaction to take place at the bridge site (Figure SI2). Due to repulsive CO*-CO* interactions, the incremental binding free energy for CO* decreases with CO* coverage (Figure SI3). The incremental binding free energy for four CO* molecules considering the most stable configurations are -1.34 eV, -0.93 eV, -0.75 eV, and -0.46 eV, respectively. Thus the driving force for further CO* adsorption is smaller at high CO* coverage. It is striking that at 0 V-RHE and 75% CO* coverage, OH* binds slightly stronger to the empty fourth site than CO* (by 0.02 eV). Thus OH* can displace the 4th CO*.

The CO* spectator coverage at experimental conditions can also be limited due to reduction of CO* to CHO* or COH*, lowering the CO* coverage. CHO* is more stable than COH* on the RuO_2 (110) surface by 0.22 eV to 0.45 eV for different CO* coverages. At 0 V-RHE, the reduction of one of CO* to CHO* is energetically uphill by 1.34 eV, 0.63 eV, 0.73 eV, and 0.03 eV for CO* coverage of 25%, 50%, 75%, and 100%, respectively. This indicates, that complete poisoning of the catalyst surfaces is not favorable. On the contrary, CO* spectators will not be removed by reduction even with application of moderate reducing potential if the coverage is low (~25%). 50% and 75% CO* coverage might be observed under CO2RR conditions, due to kinetic barriers of CO* protonation and transient evolution of CO from CO2RR. Slow transport of CO away from the catalyst will eventually leave the catalyst surface with high CO* coverage[37] as might be the case in a previous experimental study[11].

Previous studies by Popic et al. and Qu et al. employing pure ruthenium oxide electrocatalyst[9,10] have not reported any CO detected as a product. We deduce that these experimental results observing methanol as the primary product, might have a catalyst surface with low to medium CO* coverage if only a very small quantity of CO is produced and stays bound to the active site[9,10]. On the contrary, experiments by Spataru et al.[11] observe hydrogen and formic acid as dominant products along with methanol, methane and CO. It can be contemplated that the presence of CO at 30 to 200 ppm[11] in the solution comes from CO escaping the catalyst surface when a high CO* coverage is reached.

3.2. Hydroxylation with CO* spectator

CO_2 is often reduced in aqueous electrolytes. Hydroxylation of active sites is energetically downhill and spontaneous at the bridge site of RuO_2 (110) surface (Figure 1). Any available bridge site is expected to be hydroxylated at 0 V-RHE. OH* needs to be removed from the active site for CO2RR to proceed. Thus OH* removal can become a thermodynamic limiting step. Interactions between CO* and OH* are attractive for 25% to 50% CO* coverage, making OH* binding is stronger in presence of CO* spectators (Figure 1).

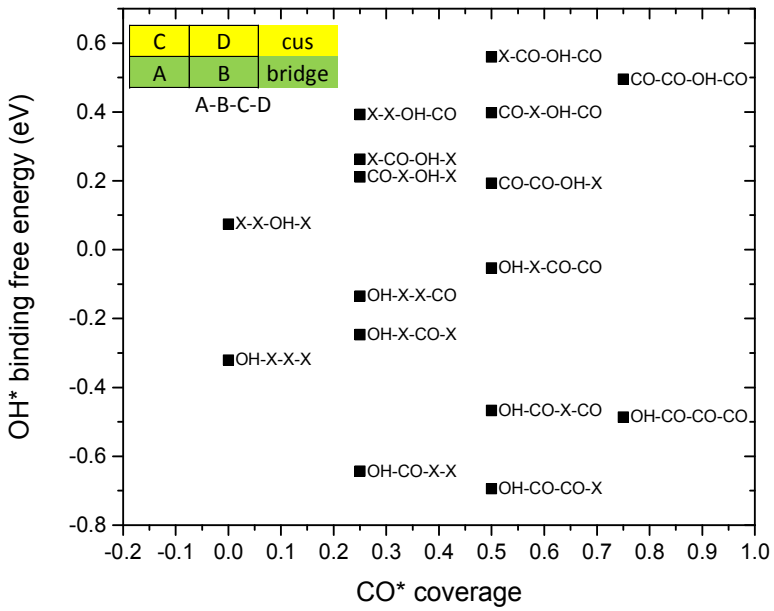

Figure 1: OH binding energy as a function of CO* coverage and spatial distribution of CO* adsorbates. As depicted in the inset, the distribution of OH* and CO* at the two bridge and two cus sites consecutively are used as label, where X denotes an unoccupied site.*

Investigations of the adsorbate binding free energy on the RuO_2 (110) surface at bridge and cus sites reveal that oxygen coordinated adsorbates like OH* bind significantly stronger to the bridge sites compared to cus sites (Figure 1). The relative preference for bridge sites is less pronounced for CO* (Figure SI3). The binding energy for OH* at different CO* spectator configurations and binding sites are presented in Figure 1 showing favored bridge site binding of OH* over cus site binding. For example, the binding energy of OH* at bridge and cus sites are -0.32 eV and +0.08 eV, respectively, while these values for CO* is -1.34 eV and -1.16 eV (w.r.t. CO molecule). This observation helps to understand the distribution of spectating CO* in bridge and cus sites under reaction conditions. Key CO2RR intermediates on oxide surfaces like OCHO*/HCOOH*/H_2COOH*, etc., are all O-coordinated. If a mixture of CO* and O-coordinated intermediates are present on the catalyst surface, CO2RR intermediates would preferentially occupy the bridge sites and the bi-dentate coordination will be preferred over mono-dentate binding. For example, three CO* and one OH* adsorbate can be distributed such that OH* can occupy a bridge site or it can occupy a cus site. The configuration with OH* in bridge site has ~1 eV lower free energy than the configuration with OH* in cus site (Figure 1). This is critical in effective CO2RR catalysis on the RuO_2 (110) surface.

Reaction path thermodynamics shows that bridge site CO2RR is not only energetically preferred but also has lower thermodynamic onset potential. For example, at 75% CO* coverage, OCHO* is unlikely to form at the cus site (binding free energy of +0.95 eV) but bridge site occupation as a mono-dentate adsorbate is feasible (binding free energy of -0.13 eV. The preferred CO* spectator configurations important for CO2RR at 0%, 25%, 50%, 75% CO* coverage are given in Figure 2 (a)-(d). Other free bridge sites and cus sites can be occupied by CO2RR/HER adsorbates as portrayed in Figure 2(e)-(i). OCHO* and H_2COOH* adsorbate binds as bi-dentate adsorbate if adjoining bridge and cus sites are not occupied by CO* spectators (Figure 2 (e) and (h)). These adsorbates are mono-dentate at high CO* coverage (Figure 2 (f)). Adsorbates like H_2CO* (Figure 2(j)) and HCOOH* (Figure 2 (g)) are always mono-dentate but reaction intermediate can consist of a pair of adsorbate like H_3CO*+OH* (Figure 2(i)).The priority of O-atom coordinated CO2RR intermediates at bridge site is not valid for HER and HER can proceed even at cus site, while bridge sites are hydroxylated. Therefore, HER thermodynamic analysis is done for variety of spectators.

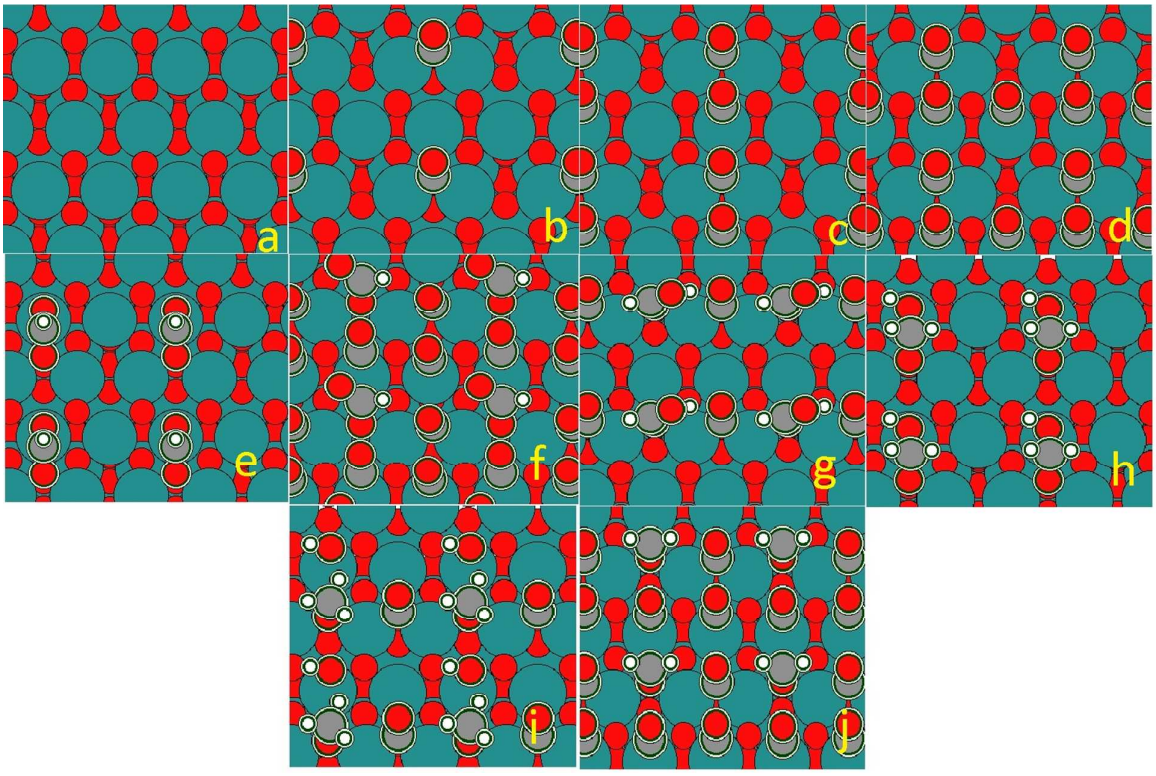

Figure 2: Simulated RuO_2(110) surface with two bridge sites and two cus sites available. Bridge sites are coordinated to two ruthenium atoms, and cus sites are on top of ruthenium atoms. (a) all sites empty. (b) one bridge site have CO. (c) one bridge site and one cus site have CO*. (d) one bridge site and two cus sites have CO*. (e) bi-dentate OCHO* bound through one bridge and one cus site. (f) OCHO* in mono-dentate configuration in bridge site with three CO* spectators occupying all*

other sites. (g) HCOOH at the bridge site with CO* in the other bridge site. (h) H_2COOH* in bi-dentate configuration. (i) H_3CO*+OH* intermediate with one bridge site CO* spectator (j) H_2CO* in bridge site with two cus site and one cus site CO* spectators. The actual unit cell in simulation is given in Figure SI1.*

3.3. CO_2 activation: OCHO* vs COOH*

From a purely thermodynamic point of view, the free energy diagrams identifies which reaction intermediate is most favorable at a particular electron transfer step. For example, if OCHO* is more stable than COOH* at 0 V-RHE, it will remain the preferred intermediate at an applied reducing potential (Figure 3(a)). A proton transfer to CO_2 molecules in the solvated phase creates both the intermediates. The free energy is lowered by the equal amount due to an applied reducing potential. OCHO* is a bi-dentate adsorbate if adjacent sites are available. At 0% and 25% CO* coverage, OCHO* binds through one bridge and one cus site (Figure 2(e)). Presence of CO* in an adjacent bridge site strengthens the OCHO* binding at low (25%) CO* coverage compared to bare catalyst surface (Figure 3(a)). At 50% CO* coverage, OCHO* can bind through one bridge and one cus site or through two cus sites depending upon the CO* distribution. On a bare surface, OCHO* occupying the bridge+cus sites have a binding free energy of -0.81 eV. It is interesting to note that the configuration with bridge+cus distribution of CO* spectators continue to be the more stable than bridge+bridge configuration when OH* or OCHO* are present on the surface. It can be argued that at a level of 50% coverage, CO2RR will occur through a combination of bridge and cus sites and OCHO* stays bi-dentate. 75% CO* coverage compel OCHO* to be mono-dentate (Figure 2(f)), reducing the binding free energy significantly. Albeit, the 2*cus+bridge configuration of CO* adsorbates lets OCHO* adsorb at the bridge site, which is significantly more favorable than the cus site adsorption. Thus, in the presence of OCHO*, the 2*cus+bridge configuration of the CO* spectators is more stable.

It should be noted that trends in COOH* and OCHO* binding free energy at different CO* adsorbate configuration are similar and maintain their relative position in the free energy diagram. Figure 3(a) shows that OCHO* intermediate is much stronger bound to the active site than COOH*, regardless of spectator coverage. Consequently, the CO2RR pathway proceed preferentially through OHCO* and other O-coordinated adsorbates at all CO* coverages. The other (unwanted) intermediate after the 1st proton transfer step is H* (Figure 3(a)).

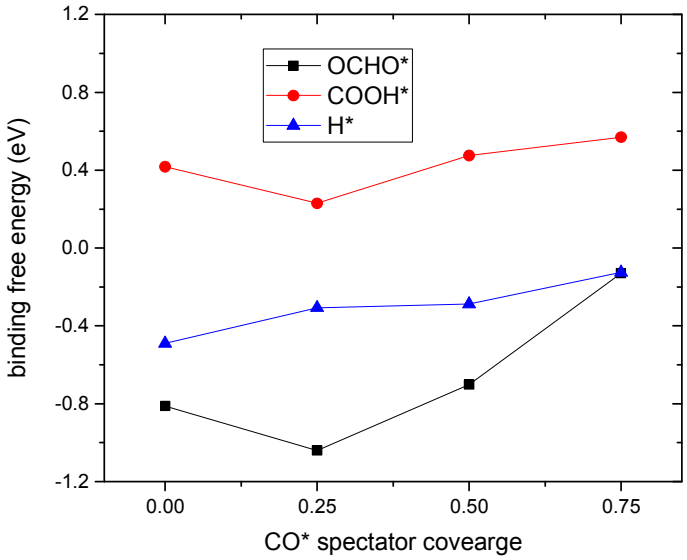

(a)

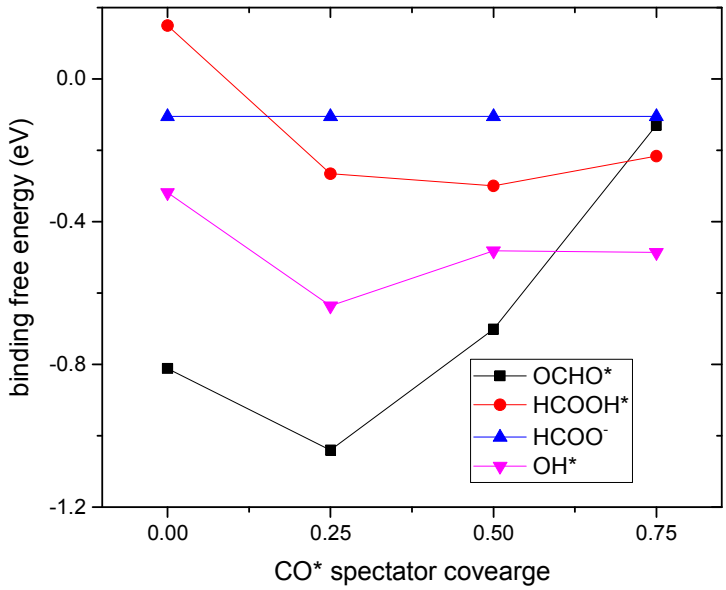

(b)

Figure 3: Effect of CO coverage on binding energy of (a) intermediates formed by the 1st proton transfer*/OCHO*/COOH*; (b) HCOOH* and OH* at the available bridge site (or bridge+cus site for OCHO*) and free energy for deprotonated formic acid in solution.*

3.4. Selectivity of CO2RR vs. HER

The spectator adsorbate interaction between CO* and H* is repulsive and H* binding weakens with higher CO* coverage (Figure 3(a)). Substantially weaker binding of H* than OCHO* facilitate selectivity of CO2RR over HER[20]. For CO* coverages 0-50%, OCHO* is stronger bound to the catalyst surface than H* by 0.31-0.73 eV (Figure 2 (a)). The binding free energy difference is over 1 eV for a coverage of 50% CO* occupying all the bridge sites (Figure SI4). Because H* is a prerequisite for HER, we thus find the best selectivity for CO2RR at 50% CO* coverage. For high (75%) CO* coverage, owing to the aforementioned destabilization of OCHO*, H* is equally probable to form (Figure 3(a)) at bridge sites (binding energy difference of 4 meV between H* and OCHO*). For 75% coverage and cus site adsorption, H* is remarkably favored by 0.32 eV over OCHO* at cus sites (Figure SI5). At high CO* coverage, RuO_2 electrocatalysts should therefore show less selectivity towards CO2RR and evolve significant amounts of hydrogen.

RuO_2(110) bridge sites, when vacant, are hydroxylated in aqueous solution due to negative binding free energy of OH* at the bridge site at 0 V-RHE (Figure 1). Hydroxylation of cus sites is not energetically favorable at 0 V-RHE and HER can proceed at the cus site. For 0% CO* coverage and hydroxylated bridge sites, the H* binding free energy at the cus site is +0.33 eV, i.e. HER requires a reducing potential of -0.33 V-RHE (Table 2). However, the OH* removal potential for clean RuO_2(110) surface bridge site is -0.32 V-RHE. Once OH* is removed, on an otherwise empty surface, the H* binding free energy at the cus site is +0.22 eV. H* binding at cus site (with H* spectators at all bridge site) is +0.41 eV. The surface coverage, onset potential and the reaction site might vary, but these binding free energies suggest that at very low CO* coverage, only HER is active at reducing potential up to -0.32 V-RHE utilizing both bridge and cus sites. Schematics of few such spectator configurations (within the 2x2-model catalyst surface) for HER mechanism and predicted onset potentials are provided in Table 2.

*Table 2: Calculated thermodynamic onset potential [V-RHE] for HER at bridge and cus sites with different spectator species on RuO_2 (110); yellow represents a cus site and green represents a bridge site. OH, CO, H are possible spectators and X is the absence of any of them. * is the site considered for HER.*

Configurations															
cus	X	*		CO	*		X	*		X	*		CO	*	
bridge	OH	OH		CO	OH		H	H		CO	X		CO	X	
HER onset [V-RHE]	-0.33			-0.56			-0.41			-0.26			-0.22		
cus	X	*		*	X		X	X		*	X		OH	*	
Bridge	OH	CO		X	X		CO	*		CO	CO		OH	OH	
HER onset [V-RHE]	-0.39			-0.22			-0.31			-0.41			-0.56		
cus	X	X		CO	X		CO	*		CO	CO				
Bridge	*	X		CO	*		CO	CO		*	CO				
HER onset [V-RHE]	-0.49			-0.29			-0.63			-0.13					

Easy availability of CO_2 in solution phase can prevent HER by formation of OCHO* in 2*cus or bridge+cus bi-dentate configuration due to higher stability than H* (Figure 3(a)). The binding free energy of OCHO* in weak binding cus site (2*cus configuration) with bridge sites filled by OH* is -0.71 eV, and when bridge sites are filled with a mixture of OH* and CO*, the OCHO* binding free energy is -0.70 eV. In comparison, H* binding is +0.33 eV and +0.39 eV for similar bridge site spectator configuration, respectively.

For 25% CO* coverage, the attractive adsorbate-adsorbate interaction between CO* and OH* at bridge sites makes OH* removal from bridge much more difficult (-0.64 V-RHE). Again bi-dentate OCHO* is very stable with a binding free energy of -1.04 eV at 25% CO* coverage. The H* binding free energy at the cus site (OH* and CO* being present at bridge sites) is +0.39 eV, cancelling significant HER activity. A similar argument for subdued HER activity holds for 50% CO* coverage (all the bridge site occupied (Figure SI4)), where all cus sites are available for adsorption. H* and OCHO* have binding free energy of +0.41 eV and -0.69 eV respectively (Table SI4). On the other hand, in the more favorable configuration, the CO* adsorbates are distributed between bridge and cus sites and the other bridge site is occupied by OH*. H* binding free energy at the cus site is +0.56 eV but the bridge OH* removal is estimated at -0.48 V-RHE. H* binding free energy at a free bridge site with 50% CO* coverage is -0.29 eV and that at cus site is +0.26 eV. Consequently, HER can progress through bridge or cus sites at ~-0.3 V-RHE (Table 2) except when OCHO* forms occupying both the bridge and cus site. This analysis shows that up to 50%

CO* coverage is expected to allow little HER activity if OCHO* forms rapidly. For the 2*bridge+cus CO* configuration (75% coverage), H* binding is very weak (+0.63 eV), while for 2*cus+bridge configuration, H* binding free energy is near ideal at +0.03 eV but hydroxylation of active site block HER above -0.48 V-RHE.

3.5. Impact of CO* coverage on CO2RR intermediate binding

Six of the CO* coverage configurations (Figure SI2) are picked for analysis of the CO2RR reaction mechanism – 0% CO* coverage, 25% CO* coverage (bridge site), 50% CO* coverage (all bridge sites). 50% CO* coverage (neighboring bridge and cus sites), 75% CO* coverage (2*bridge+cus sites), 75% CO* coverage (bridge+2*cus sites). Multisite adsorbates like H_3CO^* + OH*, which occupy two bridge sites in absence of CO* spectator and a combination of bridge+cus site for 25% and 50% CO* coverage. 75% CO* coverage only allows single site adsorbates. Some CO2RR adsorbates like OCHO* and H_2COOH^* can attach to the catalyst surface through one or two active sites, due to the molecular geometry. Such bi-dentate adsorbates are allowed to remain so for 0-50% CO* coverage. Lack of multiple neighboring vacant active sites forces them to be mono-dentate at 75% CO* coverage.

A previous study has shown that binding free energy of O-atom coordinated CO2RR reaction intermediates scale with OH* binding free energy on oxide catalysts surfaces[20]. Hence the strong spectator adsorbate interaction between CO* and OH* is expected to be valid for other O-atom coordinated CO2RR intermediates as well. Adsorbate binding energy diagrams at 0 V-RHE (Figure 4) for CO* configurations dominant at 0%, 25% (bridge site), 50% (bridge + cus sites) at 75% coverage (bridge + 2*cus sites) are used to obtain key conclusions here. Reaction intermediate free energy diagrams with two other CO* coverage configurations are provided in the supporting information (50% coverage with all bridge sites occupied (Figure SI4) and 75% coverage with on cus site free (Figure SI5)). Binding energy of an adsorbate can change from both electronic interaction with spectators as well as modifications in adsorption geometry.

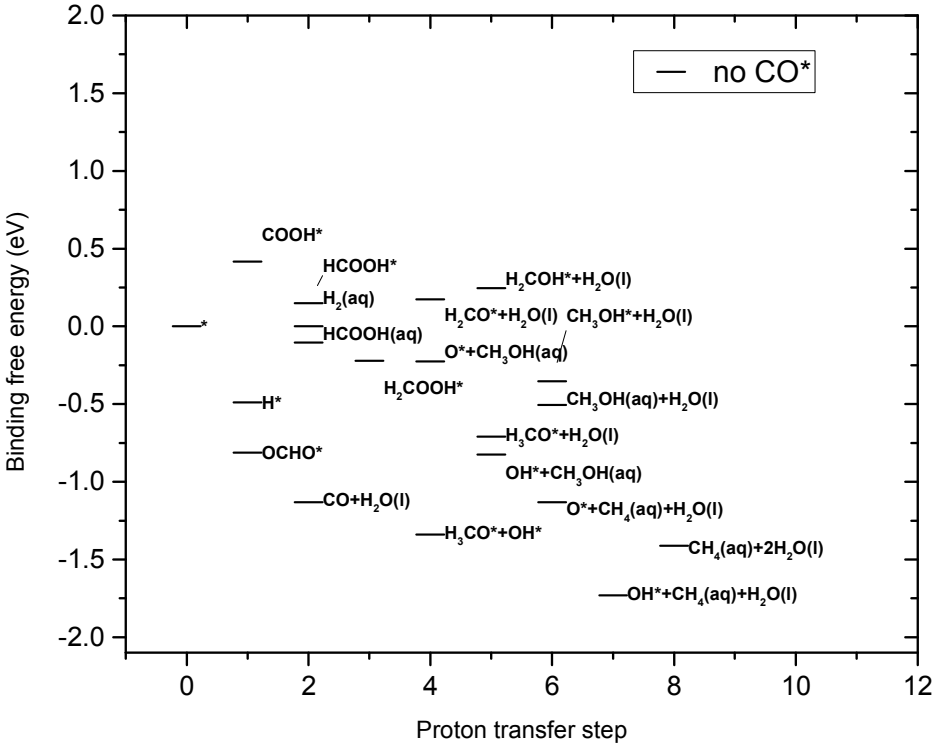
no CO*
Binding free energy (eV)
Proton transfer step
COOH*
HCOOH*
H2(aq)
*
HCOOH(aq)
H*
OCHO*
CO+H2O(l)
H2COH*+H2O(l)
H2CO*+H2O(l)
CH3OH*+H2O(l)
O*+CH3OH(aq)
H2COOH*
CH3OH(aq)+H2O(l)
H3CO*+H2O(l)
OH*+CH3OH(aq)
O*+CH4(aq)+H2O(l)
H3CO*+OH*
CH4(aq)+2H2O(l)
OH*+CH4(aq)+H2O(l)

(a)

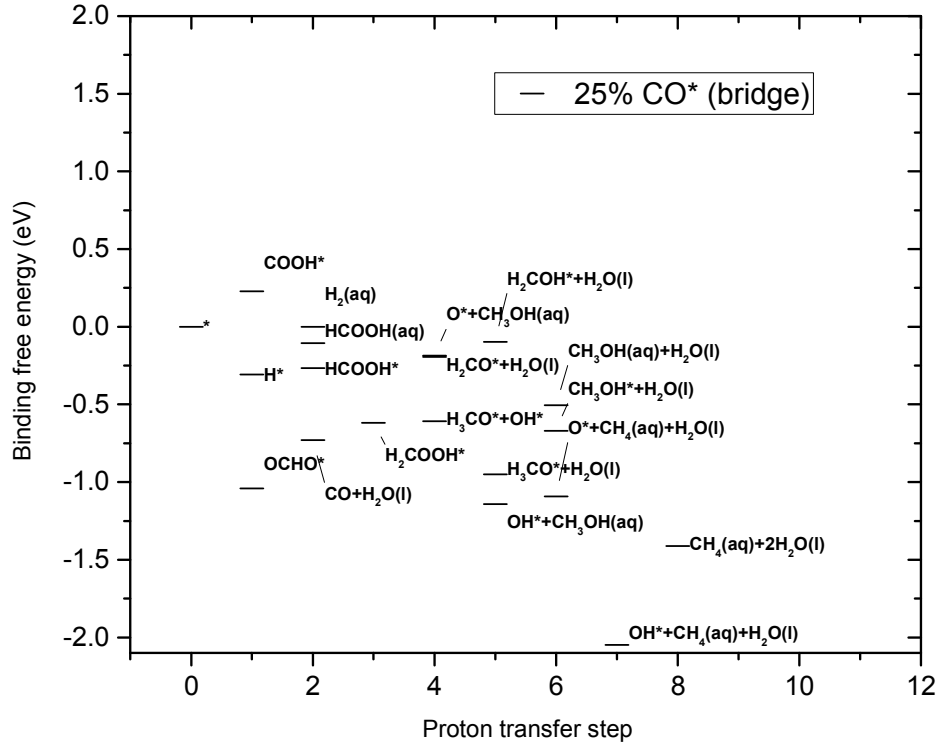
25% CO* (bridge)
Binding free energy (eV)
Proton transfer step
COOH*
H2(aq)
*
HCOOH(aq)
H*
HCOOH*
OCHO*
CO+H2O(l)
H2COH*+H2O(l)
O*+CH3OH(aq)
H2CO*+H2O(l)
CH3OH(aq)+H2O(l)
CH3OH*+H2O(l)
H3CO*+OH*
O*+CH4(aq)+H2O(l)
H2COOH*
H3CO*+H2O(l)
OH*+CH3OH(aq)
CH4(aq)+2H2O(l)
OH*+CH4(aq)+H2O(l)

(b)

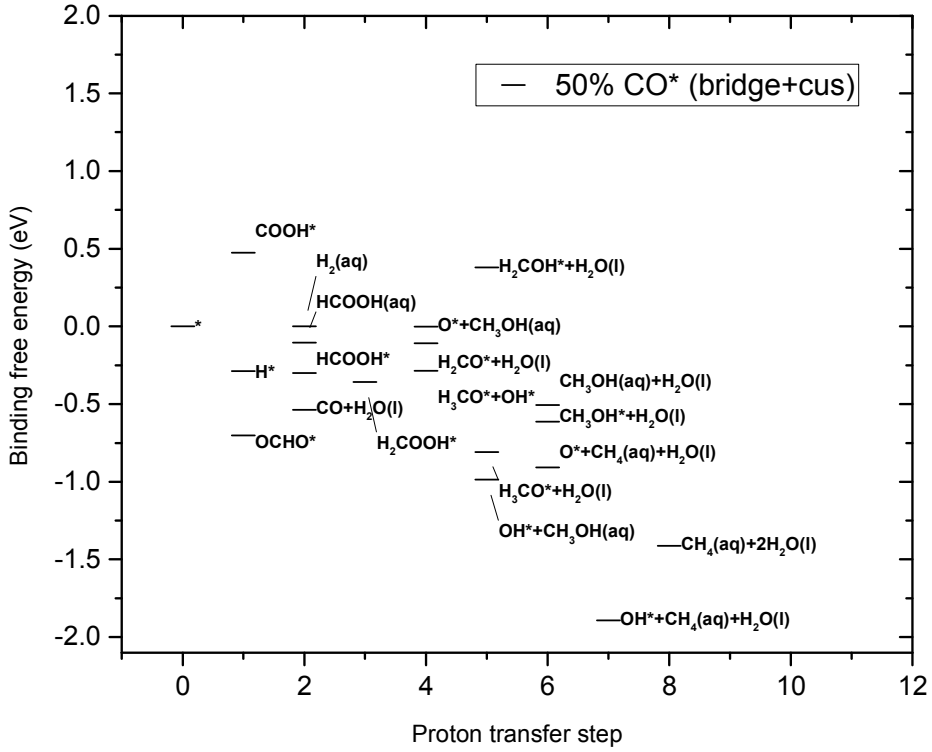
50% CO* (bridge+cus)
Binding free energy (eV)
Proton transfer step
COOH*
H2(aq)
HCOOH(aq)
*
H*
HCOOH*
CO+H2O(l)
OCHO*
H2COOH*
H2COH*+H2O(l)
O*+CH3OH(aq)
H2CO*+H2O(l)
CH3OH(aq)+H2O(l)
H3CO*+OH*
CH3OH*+H2O(l)
O*+CH4(aq)+H2O(l)
H3CO*+H2O(l)
OH*+CH3OH(aq)
CH4(aq)+2H2O(l)
OH*+CH4(aq)+H2O(l)

(c)

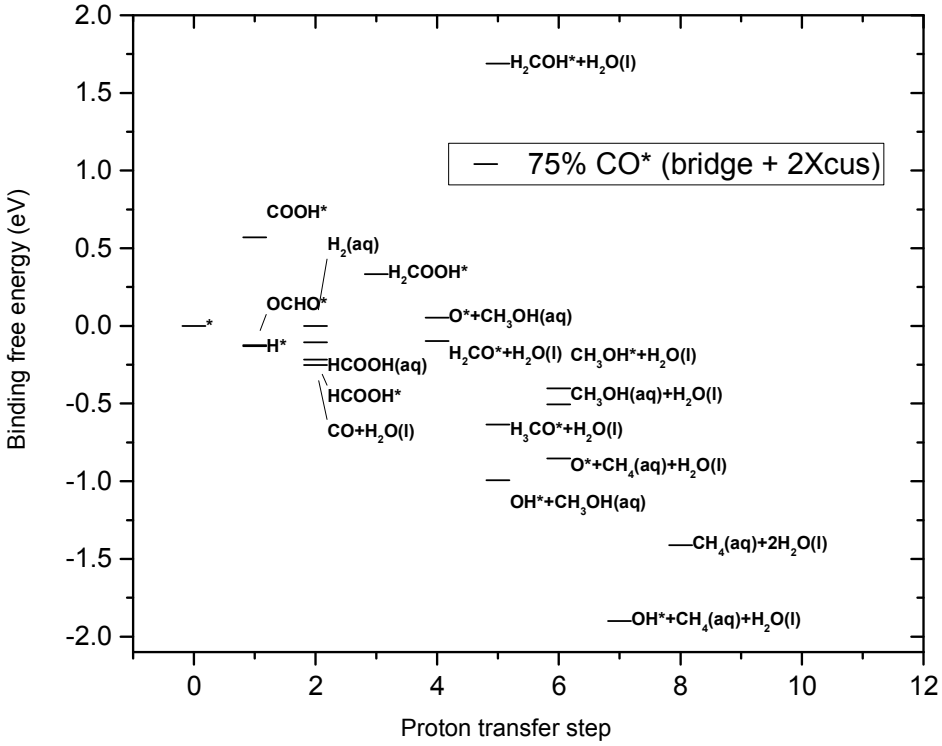
75% CO* (bridge + 2Xcus)
Binding free energy (eV)
Proton transfer step
H2COH*+H2O(l)
COOH*
H2(aq)
H2COOH*
OCHO*
*
H*
HCOOH(aq)
HCOOH*
CO+H2O(l)
O*+CH3OH(aq)
H2CO*+H2O(l)
CH3OH*+H2O(l)
CH3OH(aq)+H2O(l)
H3CO*+H2O(l)
O*+CH4(aq)+H2O(l)
OH*+CH3OH(aq)
CH4(aq)+2H2O(l)
OH*+CH4(aq)+H2O(l)

(d)

Figure 4: Free energy diagram of possible reaction intermediates for HER/CO2RR at four different coverages of CO spectators – (a) 0% (b) 25% utilizing bridge sites (c) 50% utilizing half of bridge and cus sites (d) 75% utilizing all cus and half of bridge sites.. The sites occupied by spectator CO* molecules are indicated. Adsorbate labels are on the right of the data point and adjusted in the y-direction to avoid superposition without changing the relative position between intermediates formed at the same electron transfer step.*

3.6. Impact of CO* coverage on CO2RR

The free energy diagram of reaction intermediates helps to identify which reaction intermediate is most favorable at a particular electron transfer step, and to determine the reaction mechanism. The H*/OCHO* binding free energy correlation helps us understand the HER/CO2RR selectivity; the HCOOH* binding free energy w.r.t solvated formic acid in solution (Figure 3(b)) dictates whether formic acid is the major product or higher proton transfer products like methanol is dominant. If the catalyst surface fails to bind formic acid molecules to the active site, it will escape into solution in a solvated form, rendering further hydrogenation difficult. HCOOH* being O-coordinated like OH*, the trend in the binding free energy variation at different CO* coverage are similar for these adsorbates (Figure 3 (b)). Adsorbate-adsorbate interaction effects inducing stronger OH* binding can open up the possibility of methanol/methane as product as seen in the case of partial CO* coverage.

If the formic acid molecule fails to bind at the catalyst site, H_2COOH* is expected to form by application of an additional electrochemical driving force (equivalent to the stability of deprotonated and solvated formic acid compared to surface bound HCOOH*). However, the electrolyte needs to be saturated with formic acid to supply protonated formic acid molecules. Nevertheless, the accessibility requirement of solvated HCOO- and two protons close to the active site simultaneously suggests the kinetics will be extremely slow stopping further reduction. Absence of any CO* coverage lead to release of formic acid in solution on hydrogenation of OCHO*.

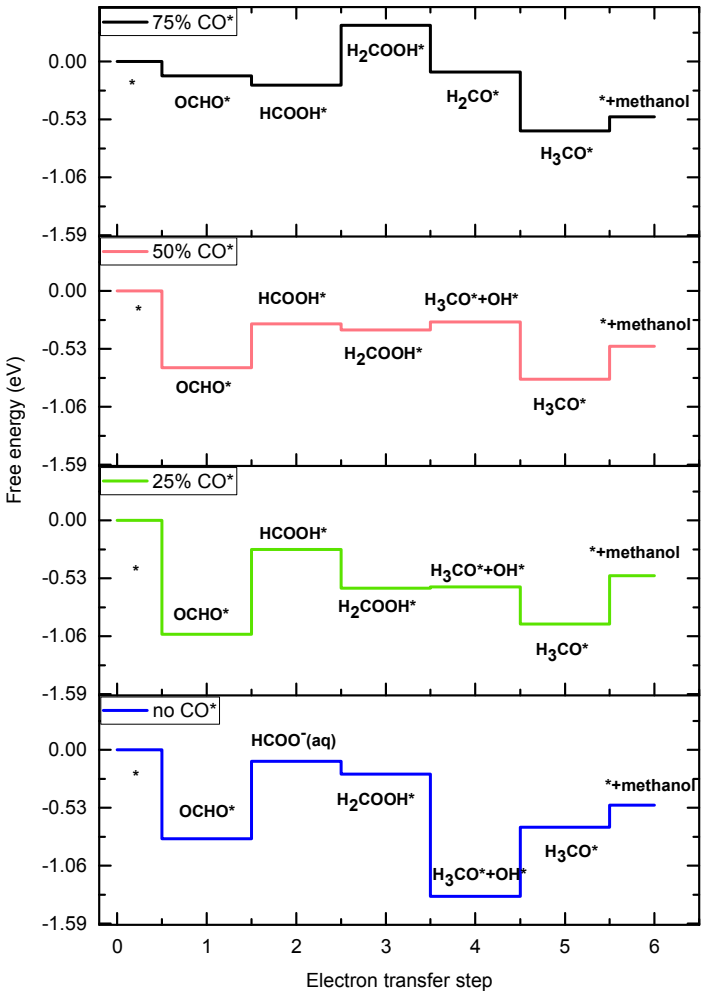
75% CO*
0.00
-0.53
-1.06
-1.59
*
OCHO*
HCOOH*
H2COOH*
H2CO*
H3CO*
*+methanol
50% CO*
0.00
-0.53
-1.06
-1.59
*
OCHO*
HCOOH*
H2COOH*
H3CO*+OH*
H3CO*
*+methanol
25% CO*
0.00
-0.53
-1.06
-1.59
*
OCHO*
HCOOH*
H2COOH*
H3CO*+OH*
H3CO*
*+methanol
no CO*
0.00
-0.53
-1.06
-1.59
*
OCHO*
HCOO-(aq)
H2COOH*
H3CO*+OH*
H3CO*
*+methanol
Free energy (eV)
0
1
2
3
4
5
6
Electron transfer step

(a)

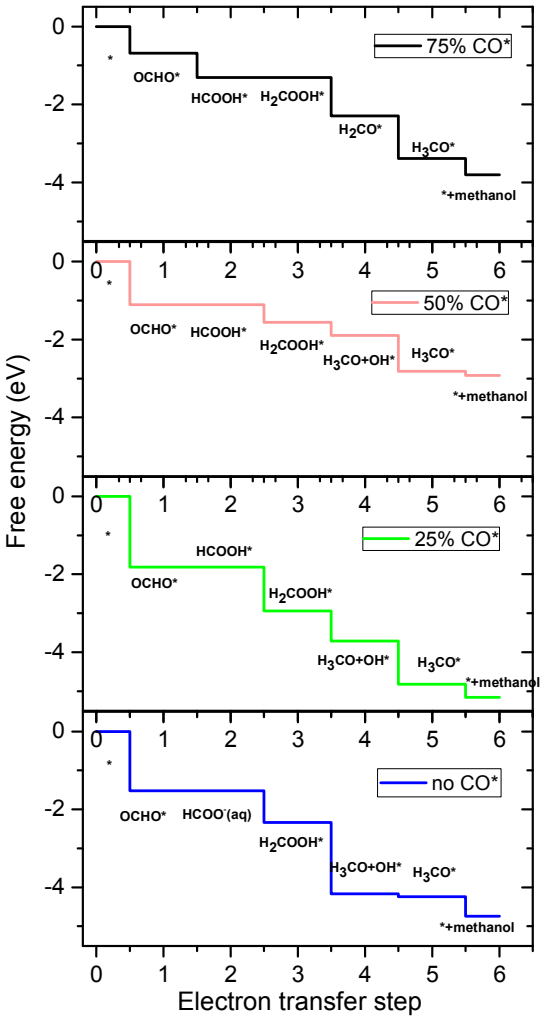

(b)

Figure 5: The thermodynamic path for methanol evolution at bridge site with 0%, 25%, 50%, 75% CO spectator coverage at (a) 0 V-RHE and (b) at the respective methanol onset potential of -0.71, -0.78, -0.4, -0.55 V-RHE. A downward step signifies no reducing potential required for forward reaction and upward step mark need for proportional reducing potential for propelling the reaction step.*

We proceed to consider formic acid in solution as a possible intermediate/product formed on OCHO* activation (Figure 5). This step leads to either surface bound HCOOH* or formic acid in solution. For CO* coverages of up to 50%, protonation of OCHO* is energetically uphill (Figure 3(b) and Figure 5(a)) forming HCOOH* on CO* covered surfaces and formic acid in the absence of CO*. This large increase in free energy requires a proportionately large reducing potential to be applied for the reaction to proceed. So OCHO* formation can reduce the HER activity in the absence of CO* simply by blocking the active sites as previously discussed. At 75% CO* coverage, OCHO* and HCOOH* are both mono-dentate. The formation of

HCOOH* from OCHO* is downhill in energy for 75% coverage (Figure 3(b)). Binding free energy of HCOOH* w.r.t. solvated formic acid in liquid water is ~0.1 eV, which is small enough for a large fraction of adsorbates to escape into solution instead of forming HCOOH* (Figure 3(b)). Weakening of the OCHO* adsorbate binding reduces the thermodynamic onset potential requirement to only –0.02 V-RHE. Therefore, at this CO* coverage, we expect a high turnover of formic acid at very low over potential, in good agreement with Spataru et. al. who observed this at only ~-0.13 V-RHE[11] and pH 3.9.

Investigations of the most probable methanol formation pathways at different CO* coverage using free energy diagrams enables us to identify the electron transfer steps requiring large reducing potentials to go forward. The preferred pathway has been established to be as following for CO* coverage ≤50%.

$$* + CO_2\,(aq) + (H^+ + e^-) \rightarrow OCHO* \quad (1)$$

$$OCHO* + (H^+ + e^-) \rightarrow HCOOH* \text{ or } OCHO* + (H^+ + e^-) \rightarrow HCOO^-\,(aq) \quad (2)$$

$$HCOOH^*\,(aq) + (H^+ + e^-) \rightarrow H_2COOH* \text{ or } HCOO^-\,(aq) + (H^+ + e^-) \rightarrow H_2COOH* \quad (3)$$

$$H_2COOH* + (H^+ + e^-) \rightarrow H_3CO* + OH* \quad (4)$$

$$H_3CO*+OH* + (H^+ + e^-) \rightarrow H_3CO* + H_2O\,(l) \quad (5)$$

$$H_3CO* + (H^+ + e^-) \rightarrow H_3COH(aq) \quad (6)$$

The lack of more than one active site for 75% CO* coverage forces the reaction pathway to go through H_2CO* instead of $H_3CO*+OH*$ adsorbates (Figure 5).

$$H_2COOH* + (H^+ + e^-) \rightarrow H_2CO* + H_2O\,(l) \quad (4a)$$

$$H_2CO*+ (H^+ + e^-) \rightarrow H_3CO* + H_2O\,(l) \quad (5a)$$

Formation of OCHO* by CO_2 protonation is downhill at 0 V-RHE for all CO* coverages. Reduction of the H_2COOH* intermediate (Figure 5 and Figure 4 (a)) is either downhill of slightly uphill (0.07 eV for 50% bridge+cus CO* coverage). Formation of H_3CO* is downhill, except in absence of any CO* coverage. In the absence of any spectators, H_3CO* and OH* can both occupy bridge sites. Stronger OH* binding energies require a large reducing potential for removal. Overall, OCHO* activation for 0% CO* coverage (0.71 eV), 25% CO* coverage (0.78 eV), 50% CO* coverage (0.4 eV) and H_2COOH* formation at 75% CO* coverage (0.55 eV) are the thermodynamically most difficult steps (Figure 4 (a)). Thus application of a reducing potential same as the onset potential for these elementary steps automatically makes all other steps downhill as represented in Figure 4(b).

Similar to the OCHO* adsorbate, H_2COOH* is also bi-dentate when two contiguous bridge and cus sites are available (Figure 2 (e),(h)); as is the case for CO* coverages up to 50%. Forcing H_2COOH* to be mono-dentate at 75% CO* coverage, makes it difficult (free energy increase of 0.6 eV more than 50% CO* coverage) to reduce HCOOH* forming H_2COOH* (Figure 5(a)). Consequently, this becomes the elementary proton transfer step, necessitating the most reducing potential. Due to interactions with spectating CO*, the stability of different intermediates change differently causing reaction step height (free energy change) to vary as well. The relative ΔG shift of these proton transfer step from intermediate binding energy variation due to CO* spectator interaction is provided in Figure SI6. Changing the CO* coverage modifies the potential needed to drive the elementary steps forward, but OCHO* activation remians the most difficult step for CO* coverage 50% or lower (Figure 5(a)).

OH* removal is not a limitation for CO2RR for any CO* coverages, except 50% (Figure SI6), where OH* removal needs a reducing potential 80 meV lower than OCHO* protonation. For CO* spectator coverage of 25% to 75%, methane and methanol evolution onset potential is close to OH* removal potential (Figure 6). The magnitude of change in overall onset potential for methanol is not as abrupt as that observed for formic acid and hydrogen evolution (75% coverage). Observable methanol evolution at different CO* coverages will therefore be dependent on kinetic barriers and competition from hydrogen and formic acid evolution. For methane evolution, the favored pathway is identical to methanol evolution until the 5^{th} electron/proton transfer step, i.e. formation of H_3CO*, at all CO* coverages. At the 6^{th} step, methane is released by protonation on the carbon atom of the H_3CO* adsorbate, leaving an oxygen atom at the bridge site, which is eventually removed as water through two protonation steps. The thermodynamic limiting steps are identical to methanol evolution, except at 50% coverage, where the onset potential predicted of methane evolution from thermodynamic analysis is different from methanol (Figure 6). From H_3CO*, methane evolution will be preferred if C-O bond cleaving has a smaller barrier than detaching Ru-O bond.

Experimental evidence[8,9] points to methanol formation having a smaller barrier, as methanol has been observed to be produced in much larger quantities than methane[9–11]. Popic et. al. observed up to 30.5% product efficiency for methanol at ~ -0.12 V-RHE, while no CO has been reported to be present. Conversely, Spataru et al. report excellent HCOOH/H_2 evolution with CO as minority product at similar potential on RuO_2 electrode. These experimental results directly correlate to our conclusion that, moderate CO* coverage aid in methanol evolution and high CO* coverage leads to HCOOH/H_2 at very low potential.

Our simulation model does not explicitly consider pH effects. The discrepancy between observed and predicted methanol onset potential can originate from variations in CO* coverage, pH effects or other differences like composition and

surface structure. Preliminary work[8] by Bandi suggested strong dependence of methanol evolution efficiency on pH and observed a much better methanol efficiency in acidic solution than neutral electrolyte. The concentration of methanol in the solvent can also affect the reaction thermodynamics of methanol production. With higher concentration, free energy of methanol increases and release of methanol from H_3CO^* intermediate needs larger reducing potential.

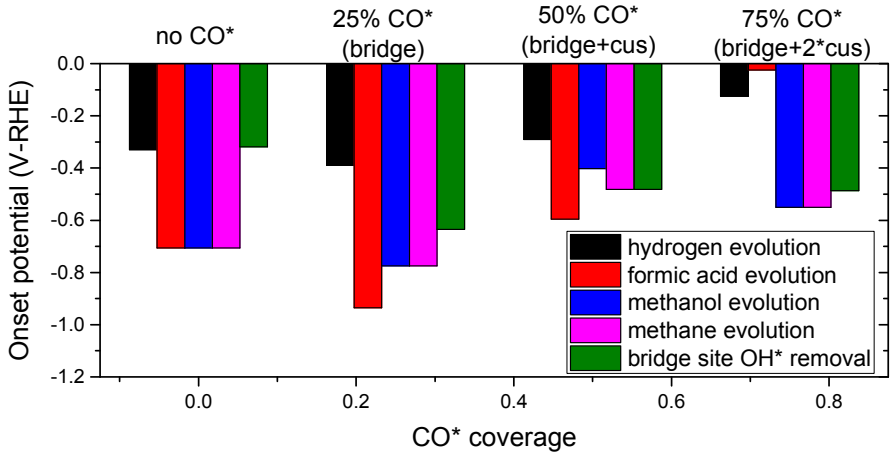

Figure 6: Onset potentials for hydrogen, formic acid, methanol, methane evolution at different CO spectator coverage. OH* removal potential at bridge site included to provide information about possible OH* blockage.*

4. Conclusions

In summary, without CO* coverage, RuO_2(110) is expected to start producing hydrogen via the cus sites (-0.33 V-RHE) with hydroxylated bridge sites. Repulsive interactions with CO* spectators destabilize H*. If the availability of CO_2 in the reaction layer and the kinetic barriers for CO_2 activation are not limiting, OCHO* is preferred over H* as the 1st proton transfer product, as seen from a purely thermodynamic perspective. Transient formation of CO* from CO2RR leads to 25% to 75% CO* coverage. A large reducing potential is required to protonate stable bi-dentate OCHO* and break one Ru-O bond at 0-50% CO* coverage. At 25% CO* coverage, methanol is expected to be the main CO2RR product, with an onset potential of -0.78 V-RHE because HCOOH* is surface bound. 50% CO* coverage is predicted to provide the best activity towards methanol formation. At this CO* coverage, the HER cannot start above -0.56 V-RHE due to bridge site hydroxylation (Table 2) while methanol formation (onset of -0.4 V-RHE) is active at the OH* removal potential (-0.48 V-RHE). At a sufficient reducing potential, the CO2RR pathway to methanol is expected to show significant activity in conjunction with little hydrogen evolution for 25%-50% CO* coverage. The 75% CO* covered surface, on the contrary, have close to ideal onset potential for formic acid production, due to weakly bound mono-dentate OCHO*. Once OH* is removed from the active site, both hydrogen and formic acid is expected to form. Suppression of HER at 50% or

lower CO* coverage by formation of OCHO* at the active sites is critically dependent on fast reaction kinetics for OCHO* formation. Good activity and selectivity obtained for CO2RR on RuO_2 catalysts are highly dependent on the CO* coverage in the reaction environment. At high CO* coverages (75%), excellent availability of CO_2 is critical for formic acid evolution. If, however, CO_2 molecules are not readily available, hydrogen is expected to be the only observable product.

Binding energy alteration of both H* and CO2RR intermediates emerging from adsorbate interaction with CO* lets us observe switching of CO2RR/HER activity and CO2RR product selectivity at the optimal CO* coverage. 25%-50% CO* coverage is most conducive for methanol formation and higher CO* coverage for formic acid evolution.

RuO_2 based electrocatalysts have been shown experimentally to hold great promise for direct conversion of CO_2 to methanol and formic acid. Based on this theoretical exploration, we show that CO* spectators hold the key to good CO2RR activity and selectivity.

Supporting Information

Additional visualizations of and explanation for CO* coverage configurations, adsorbate free energy diagrams, thermodynamic data for adsorbates and molecules, figure for methanol evolution elementary reaction step onset dependency on CO* coverage, free energy of CO* coverage configurations, visualization for all possible CO* spectator models as well as atomic position data and visualization all catalyst surface simulations are provided.

Acknowledgements

Funding from the Lundbeck foundation (grant no. R141-2013-A13204) and The Velux Foundations through V-Sustain: The VILLUM Center for the Science of Sustainable Fuels and Chemicals (Grant no. 9455) are gratefully acknowledged. The Niflheim supercomputer at DTU was used for the computations performed in this work.

References:

(1) Chu, S.; Majumdar, A. Opportunities and Challenges for a Sustainable Energy Future. *Nature* **2012**, *488* (7411), 294–303.

(2) Dunn, B.; Kamath, H.; Tarascon, J.-M. Electrical Energy Storage for the Grid: A Battery of Choices. *Science (80-.).* **2011**, *334* (6058), 928–935.

(3) Ganesh, I. Conversion of Carbon Dioxide into Methanol - A Potential Liquid Fuel: Fundamental Challenges and Opportunities (a Review). *Renew. Sustain.*

Energy Rev. **2014**, *31* (2014), 221–257.

(4) Hori, Y. Electrochemical CO2 Reduction on Metal Electrodes. In *Modern Aspects of Electrochemistry*; Springer New York: New York, NY, 2008; Vol. 42, pp 89–189.

(5) Kuhl, K. P.; Hatsukade, T.; Cave, E. R.; Abram, D. N.; Kibsgaard, J.; Jaramillo, T. F. Electrocatalytic Conversion of Carbon Dioxide to Methane and Methanol on Transition Metal Surfaces. *J. Am. Chem. Soc.* **2014**, *136* (40), 14107–14113.

(6) Peterson, A. A.; Abild-Pedersen, F.; Studt, F.; Rossmeisl, J.; Nørskov, J. K.; Lewis, N. S.; Nocera, D. G.; Hori, Y.; Kikuchi, K.; Murata, A.; et al. How Copper Catalyzes the Electroreduction of Carbon Dioxide into Hydrocarbon Fuels. *Energy Environ. Sci.* **2010**, *3* (9), 1311-1315.

(7) Peterson, A. A.; Nørskov, J. K. Activity Descriptors for CO_2 Electroreduction to Methane on Transition-Metal Catalysts. *J. Phys. Chem. Lett.* **2012**, *3* (2), 251–258.

(8) Bandi, A. Electrochemical Reduction of Carbon Dioxide on Conductive Metallic Oxides. *J. Electrochem. Soc.* **1990**, *137* (7), 2157.

(9) Popic, J. P.; Avramov-Ivic, M. L.; Vukovic, N. B.; Popić, J.; Avramov-Ivić, M.; Vuković, N.; Popic, J. P.; Avramov-Ivic, M. L.; Vukovic, N. B.; Popić, J.; et al. Reduction of Carbon Dioxide on Ruthenium Oxide and Modified Ruthenium Oxide Electrodes in 0.5 M NaHCO 3. *J. Electroanal.* **1997**, *421*, 105–110.

(10) Qu, J.; Zhang, X.; Wang, Y.; Xie, C. Electrochemical Reduction of CO_2 on RuO_2/TiO_2 Nanotubes Composite Modified Pt Electrode. *Electrochim. Acta* **2005**, *50* (16–17), 3576–3580.

(11) Spataru, N.; Tokuhiro, K.; Terashima, C.; Rao, T. N.; Fujishima, A. Electrochemical Reduction of Carbon Dioxide at Ruthenium Dioxide Deposited on Boron-Doped Diamond. *J. Appl. Electrochem.* **2003**, *33* (12), 1205–1210.

(12) Rasul, S.; Anjum, D. H.; Jedidi, A.; Minenkov, Y.; Cavallo, L.; Takanabe, K. A Highly Selective Copper-Indium Bimetallic Electrocatalyst for the Electrochemical Reduction of Aqueous CO_2 to CO. *Angew. Chemie - Int. Ed.* **2015**, *54* (7), 2146–2150.

(13) Mistry, H.; Reske, R.; Zeng, Z.; Zhao, Z. J.; Greeley, J.; Strasser, P.; Cuenya, B. R. Exceptional Size-Dependent Activity Enhancement in the Electroreduction of CO_2 over Au Nanoparticles. *J. Am. Chem. Soc.* **2014**, *136* (47), 16473–16476.

(14) Li, Y.; Cui, F.; Ross, M. B.; Kim, D.; Sun, Y.; Yang, P. Structure-Sensitive CO_2 Electroreduction to Hydrocarbons on Ultrathin Five-Fold Twinned Copper Nanowires. *Nano Lett.* **2017**, *17* (2), 1312-1317.

(15) Varela, A. S.; Schlaup, C.; Jovanov, Z. P.; Malacrida, P.; Horch, S.; Stephens, I. E. L.; Chorkendorff, I. CO_2 Electroreduction on Well-Defined Bimetallic

Surfaces: Cu Overlayers on Pt(111) and Pt(211). *J. Phys. Chem. C* **2013**, *117* (40), 20500–20508.

(16) Li, C. W.; Kanan, M. W. CO_2 Reduction at Low Overpotential on Cu Electrodes Resulting from the Reduction of Thick Cu_2O Films. *J. Am. Chem. Soc.* **2012**, *134* (17), 7231–7234.

(17) Jovanov, Z. P.; Hansen, H. A.; Varela, A. S.; Malacrida, P.; Peterson, A. A.; Nørskov, J. K.; Stephens, I. E. L.; Chorkendorff, I. Opportunities and Challenges in the Electrocatalysis of CO_2 and CO Reduction Using Bifunctional Surfaces: A Theoretical and Experimental Study of Au-Cd Alloys. *J. Catal.* **2016**, *343*, 215–231.

(18) Torelli, D. A.; Francis, S. A.; Crompton, J. C.; Javier, A.; Thompson, J. R.; Brunschwig, B. S.; Soriaga, M. P.; Lewis, N. S. Nickel-Gallium-Catalyzed Electrochemical Reduction of CO_2 to Highly Reduced Products at Low Overpotentials. *ACS Catal.* **2016**, *6* (3), 2100–2104.

(19) Karamad, M.; Hansen, H. A.; Rossmeisl, J.; Nørskov, J. K. Mechanistic Pathway in the Electrochemical Reduction of CO_2 on RuO_2. *ACS Catal.* **2015**, *5* (7), 4075–4081.

(20) Bhowmik, A.; Vegge, T.; Hansen, H. A. Descriptors and Thermodynamic Limitations of Electrocatalytic Carbon Dioxide Reduction on Rutile Oxide Surfaces. *ChemSusChem* **2016**, *9* (22), 3230–3243.

(21) Peterson, A. A.; Abild-Pedersen, F.; Studt, F.; Rossmeisl, J.; Nørskov, J. K.; Lewis, N. S.; Nocera, D. G.; Hori, Y.; Kikuchi, K.; Murata, A.; et al. How Copper Catalyzes the Electroreduction of Carbon Dioxide into Hydrocarbon Fuels. *Energy Environ. Sci.* **2010**, *3* (9), 1311.

(22) Back, S.; Kim, H.; Jung, Y. Selective Heterogeneous CO_2 Electroreduction to Methanol. *ACS Catal.* **2015**, *5* (2), 965–971.

(23) An, W.; Xu, F.; Stacchiola, D.; Liu, P. Potassium-Induced Effect on the Structure and Chemical Activity of the Cu_xO/Cu(1 1 1) ($X \leq 2$) Surface: A Combined Scanning Tunneling Microscopy and Density Functional Theory Study. *ChemCatChem* **2015**, *7* (23), 3865–3872.

(24) Cui, C.; Han, J.; Zhu, X.; Liu, X.; Wang, H.; Mei, D.; Ge, Q. Promotional Effect of Surface Hydroxyls on Electrochemical Reduction of CO_2 over SnO_x/Sn Electrode. *J. Catal.* **2016**, *343*, 257–265.

(25) Marshall, S. T.; Medlin, J. W. Surface-Level Mechanistic Studies of Adsorbate adsorbate Interactions in Heterogeneous Catalysis by Metals. *Surf. Sci. Rep.* **2011**, *66* (5), 173–184.

(26) Wang, H. Y.; Schneider, W. F. Comparative Chemistries of CO and NO Oxidation over RuO_2(110): Insights from First-Principles Thermodynamics and Kinetics. *Mol. Simul.* **2012**, *38* (8–9), 615–630.

(27) Tang, D. C.; Hwang, K. S.; Salmeron, M.; Somorjai, G. A. High Pressure

Scanning Tunneling Microscopy Study of CO Poisoning of Ethylene Hydrogenation on Pt(111) and Rh(111) Single Crystals. *J. Phys. Chem. B* **2004**, *108* (35), 13300–13306.

(28) Zhang, Y. J.; Sethuraman, V.; Michalsky, R.; Peterson, A. A. Competition between CO_2 Reduction and H_2 Evolution on Transition-Metal Electrocatalysts. *ACS Catal.* **2014**, *4* (10), 3742–3748.

(29) Kresse, G. From Ultrasoft Pseudopotentials to the Projector Augmented-Wave Method. *Phys. Rev. B* **1999**, *59* (3), 1758–1775.

(30) Kiejna, A.; Kresse, G.; Rogal, J.; De Sarkar, A.; Reuter, K.; Scheffler, M. Comparison of the Full-Potential and Frozen-Core Approximation Approaches to Density-Functional Calculations of Surfaces. *Phys. Rev. B - Condens. Matter Mater. Phys.* **2006**, *73* (3), 6–9.

(31) Norskov, J. K.; Bligaard, T.; Rossmeisl, J.; Christensen, C. H. Towards the Computational Design of Solid Catalysts. *Nat Chem* **2009**, *1* (1), 37–46.

(32) Wellendorff, J.; Lundgaard, K. T.; Møgelhøj, A.; Petzold, V.; Landis, D. D.; Nørskov, J. K.; Bligaard, T.; Jacobsen, K. W. Density Functionals for Surface Science: Exchange-Correlation Model Development with Bayesian Error Estimation. *Phys. Rev. B - Condens. Matter Mater. Phys.* **2012**, *85* (23), 235149/1-23.

(33) Butler, S. R.; Gillson, J. L. Crystal Growth, Electrical Resistivity and Lattice Parameters of RuO_2 and IrO_2. *Mater. Res. Bull.* **1971**, *6* (2), 81–89.

(34) Christensen, R.; Hansen, H. A.; Vegge, T. Identifying Systematic DFT Errors in Catalytic Reactions. *Catal. Sci. Technol.* **2015**, *5* (11), 4946–4949.

(35) Hansen, H. A.; Shi, C.; Lausche, A.; Peterson, A.; Nørskov, J. K. Bifunctional Alloys for the Electroreduction of CO_2 and CO. *Phys. Chem. Chem. Phys.* **2016**, *18* (111), 9194–9201.

(36) Nørskov, J. K.; Rossmeisl, J.; Logadottir, A.; Lindqvist, L.; Kitchin, J. R.; Bligaard, T.; Jónsson, H. Origin of the Overpotential for Oxygen Reduction at a Fuel-Cell Cathode. *J. Phys. Chem. B* **2004**, *108* (46), 17886–17892.

(37) Reuter, K.; Scheffler, M. Composition and Structure of the RuO_2 (110) Surface in an O_2 and CO Environment: Implications for the Catalytic Formation of CO_2 Karsten. *Phys. Rev. B* **2001**, *65* (3), 045407/1-11.

TOC Graphic